Journal of Vibration Engineering & Technologies (2024) 12:7009–7019
https://doi.org/10.1007/s42417-024-01295-2

ORIGINAL PAPER

A Non-uniform Equivalent Model for Free Vibration Analysis of Sandwich Composite Panels with Trapezoidal Lattice Core

Haoran Wang[1,2] · **Mengzhen Li**[1,2] · **Xiaolong Liu**[1,2]

Received: 28 October 2023 / Revised: 14 January 2024 / Accepted: 2 February 2024 / Published online: 17 March 2024
© Springer Nature Singapore Pte Ltd. 2024

Abstract

Objective Free vibration characteristics of the trapezoidal lattice sandwich composite panels are investigated based on a novel equivalent plate model.

Methods The equivalent shear modulus and the relative density of the graded lattice core are assumed to be thickness-dependent and these material properties are calculated based on the single-cell equivalence theory and the continuity assumption. Under the framework of the higher-order shear deformation theory (HSDT), the unknown displacement functions are expressed in terms of standard Fourier series and auxiliary functions to avoid discontinuities on the edges of lattice sandwich plate. Artificial spring technique is utilized to simulate arbitrary boundary conditions and the unknown coefficients in the displacement functions are obtained by Rayleigh–Ritz variational method.

Results The accuracy of the present method can be verified by comparing the obtained results with FEM results and those from literature. On this basis, a detailed parametric study concerning the effect of boundary conditions, aspect ratio a/b, tilt angle θ, and lamination schemes on the vibration frequencies of the trapezoidal lattice sandwich plate is also performed.

Keywords Trapezoidal lattice plates · Analytical modelling · Sandwich composite structures · Non-uniform equivalent model · Vibration analysis

Abbreviations

C,S,E,F	Clamped, Simply support, Elastic, Free boundary conditions
x,y,z	Coordinates axes
K_u, K_v, K_w, K_x, K_y	Spring stiffness coefficients
a, b	Short and long bases of the trapezoidal core, (m)
c	Distance between adjacent lattice core, (M)
t_0	Thickness of lattice core, (M)
θ	Tilt angle of the core, (°)
$l1$, $l2$	Length and width of a single cell, (m)
h_f, h_c	Thickness of panel and core, (m)
L_a, L_b	Length and width of sandwich panels, (m)
H	Total thickness of sandwich panels, (M)
E_1	Modulus of elasticity of the face sheets, (GPa)
G	Equivalent shear modulus, (GPa)
ρ, ρ_c, ρ_0	Relative density, core density, the density of face sheets, (kg/m^3)
M, N	Truncation numbers

Introduction

Lattice sandwich structures have drawn increasing attention in aerospace, vehicle marine, and other engineering fields due to their excellent properties such as light weight, high strength, high stiffness, high heat dissipation, outstanding design and multifunctional characteristics [1–3]. The graded lattice structures have excellent structural properties due to the changing configuration and properties of the lattice in space [4]. The graded lattice structure is connected stably, with the advantages of high modularity and strength under small strains, as well as layer-by-layer performance enhancement under large strains [5]. Currently, the mechanical

✉ Mengzhen Li
mengzhen.li@whut.edu.cn

[1] State Key Laboratory of Maritime Technology and Safety, Wuhan University of Technology, Wuhan, China

[2] School of Transportation and Logistics Engineering, Wuhan University of Technology, Wuhan, China

properties [6] and preparation [7] of metal lattice sandwich structures with different topology cores have been widely studied, but their vibration, damping, and heat-insulating panel properties still need to be further explored.

Great research efforts have been devoted to the equivalent methods for sandwich panels, shells and beams with lattice, honeycomb and corrugated core. Beiranvand and Hosseini [8] investigated the free vibration of a simply supported beam based on a new geometrically model. The free vibration characteristics of sandwich beam with honeycomb-corrugation hybrid cores were studied with the help of the homogenization method by Zhang et al. [9]. Lou et al. [10] investigated the free vibration of lattice sandwich beams by employing an equivalence model. Han et al. [11] investigated the free vibration characteristics of CFRC lattice-core sandwich cylinder by using the energy method. Zhong et al. [12] studied the time- and frequency- domain vibration characteristics of enhanced pyramid lattice sandwich panels by an equivalent downscaling method. Kwak et al. [13] investigated the free vibration of the graded arbitrary quadrilateral panels based on a new MLST shape function. Li et al. [14] studied the nonlinear free vibration characteristics of graded honeycomb sandwich cylindrical shells by adopting the multiple scales method.

Secgin and Kara [15] investigated the stochastic vibration characteristics of the composite plate based on a probabilistic methodology. Zhang et al. [16] studied the nonlinear vibration characteristics of the FG-CNTRC plates by employing meshless method. Banerjee et al. [17] used the first-order shear deformation theory to study the free vibration response of composite conical shell. Saiah et al. [18] applied the extended Halpin–Tsai approach to investigate the vibration characteristic of GRNC laminated panels. Raza et al. [19] proposed a novel computational algorithm for investigating the vibration characteristics of functionally graded panels. Liu et al. [20] used the separation method to study the vibration of three-phase composite panels. Li et al. [21] studied the vibration response of metallic sandwich plates with Hourglass lattice cores. Zhou et al. [22] proposed a theoretical method to study the free and forced vibration characteristics of simply supported Z-reinforced sandwich structures. The vibration characteristics of novel multilayer sandwich beams was researched with the help of the deformation energy based method by Li et al. [23].

Based on the aforementioned literature review, it is evident that there are currently numerous studies focusing on conventional equivalence methods and dynamic models for sandwich lattice structures. However, the methods for predicting the vibration characteristics of novel trapezoidal lattice plates are relatively rare. In present research, a new equivalent model is proposed to study the free vibration of the trapezoidal lattice sandwich composite panels based on the single-cell equivalence theory and the continuity assumption. An improved higher-order shear deformation theory is applied to derive strain energy, spring potential energy, and kinetic energy of the trapezoidal lattice sandwich panels, before the eigenvalue equation is obtained using the Rayleigh–Ritz method. Finally, the effect of boundary conditions, aspect ratio a/b, thickness, tilt angle θ, and lamination schemes on the vibration frequencies is studied in detail.

Theoretical Formulations

Trapezoidal Lattice Sandwich Composite Panels

A graded lattice sandwich composite panel with length L_a, width L_b and constant thickness h in the Cartesian coordinate system (x-y-z) has been illustrated in Fig. 1. The upper and lower panels, as well as the core material, are all made of carbon fiber-reinforced composite laminates. It is assumed that the lattice core is well bonded to the panels without relative sliding. The lattice core consists of many sets of symmetric trapezoidal laminates, assuming the size of the unit cell can be neglected compared to the overall dimensions. The specifications for the 1-direction and 2-direction of the panels and core material are as shown in Fig. 1. In this study, the artificial spring technique is used to simulate the arbitrary boundary conditions [24–26]. Three linear springs and two rotational springs are distributed along the edges of the physical middle surface. The values of spring stiffness coefficients can vary from zero to infinity, and the classical boundary conditions (such as simply supported, clamped, free boundary conditions) and elastic boundary conditions can be represented with the combinations of these linear and rotational springs.

Equivalent Model of the Trapezoidal Lattice Sandwich Composite Panels

The representative volume element (RVE) is firstly established to obtain the material parameters of the equivalent plate, as shown in Fig. 2. The upper panel and lower panel

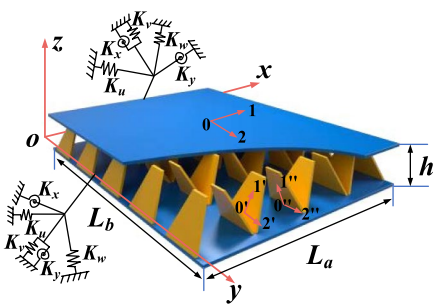

Fig. 1 A trapezoidal lattice sandwich composite panel

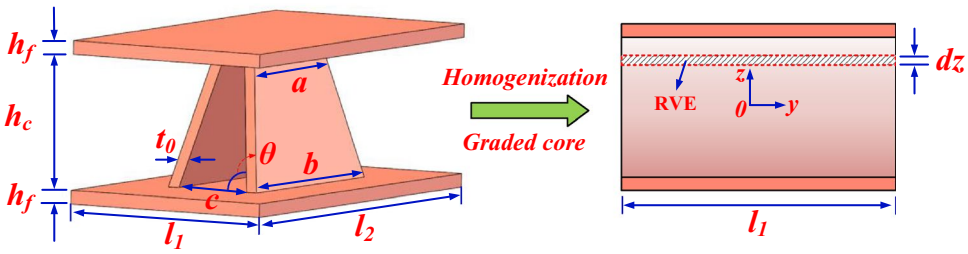

Fig. 2 Schematic illustration of a representative volume element of the trapezoidal lattice panel

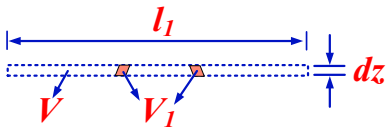

Fig. 3 The representative volume element of the lattice core

have the same thickness of h_f, while the core thickness is h_c. Normally, traditional lattice core with uniform cross-sections can be considered to have the same material properties throughout the thickness direction, and this can help to simplify the traditional lattice sandwich panels into sandwich panels with uniform isotropic cores. However, for trapezoidal lattice cores, it is assumed that the material properties of the core material vary with thickness, making the equivalent core material similar to functionally graded materials. Therefore, in order to obtain the equivalent properties of trapezoidal cores, a small thickness segment dz is taken for analysis, as shown in Fig. 2.

Relative Density of the Lattice Core

To obtain the thickness-dependent relative density of the core material, a representative volume element with a thickness of dz is analyzed, as shown in Fig. 3. The relative density of the core material can be expressed as the ratio of the mass of the core material to the volume of the entire representative volume element.

From the geometrical relationship, the relative density of the trapezoidal lattice core ρ_c can be obtained:

$$\rho_c(z) = \frac{V_1}{V}\rho_0 = \frac{2t_0}{l_1 l_2}\left(\frac{a-b}{h_c}z + \frac{a+b}{2}\right)\rho_0 \tag{1}$$

where V_1, V are the volume of the core material and that of the RVE. z represents the thickness coordinate and ρ_0 is the density of the CFRP panel.

The Equivalent Shear Modulus

It is assumed that only shear deformation is considered for the lattice core [27] [28]. It is assumed that there is a shear load p applied at the nodes of the pyramidal single cell (see Fig. 4), causing a displacement of δ in the x direction. Similarly, in the representative volume element with a thickness of dz, the upper and lower surfaces of RVE are subjected to a pair of shear forces p. It can be assumed that the lattice core in the RVE has the same width and it is taken for the force analysis, as shown in Fig. 4(b).

Based on geometric relationships and force equilibrium, we have:

$$\frac{p}{2} = F_a \cos\theta \tag{2}$$

$$\delta = \frac{\Delta l}{\cos\theta} \tag{3}$$

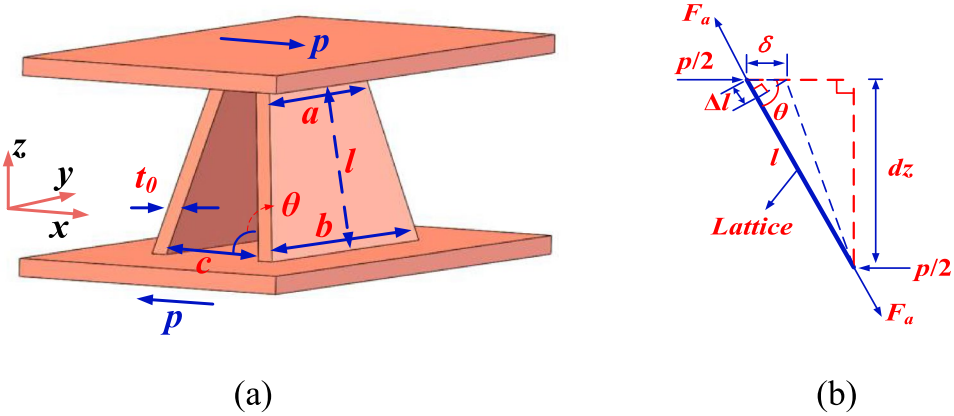

Fig. 4 **a** A graded cell under shear load; **b** Loading analysis on a single trapezoidal plate

$$\varepsilon = \frac{\Delta l}{l} = \frac{\sin\theta \Delta l}{dz} \tag{4}$$

The axial force in one trapezoidal lattice under shear load is:

$$F_a = E_1 \varepsilon t_0 w_l(z) = E_1 \varepsilon t_0 \left(\frac{a-b}{h_c} z + \frac{a+b}{2}\right) \tag{5}$$

At this point, the shear strain and shear stress of the single cell are:

$$\gamma = \frac{\delta}{dz} \tag{6}$$

$$\tau = \frac{p}{l_1 l_2} \tag{7}$$

This leads to a trapezoidal lattice core shear modulus of:

$$G = \frac{\tau}{\lambda\gamma} = \frac{2E_1 \sin\theta \cos\theta^2 t_0}{\lambda l_1 l_2}\left(\frac{a-b}{h_c} z + \frac{a+b}{2}\right) \tag{8}$$

where the correction factor $\lambda = hl_2a^2/(t_0^3 c)$ is related to the geometric configuration of the trapezoidal lattice core.

Mathematical Model of the Trapezoidal Lattice Sandwich Composite Panels

The displacement fields are constructed based on the higher-order shear deformation theory:

$$\begin{Bmatrix} u(x,y,z,t) \\ v(x,y,z,t) \\ w(x,y,z,t) \end{Bmatrix} = \begin{bmatrix} 1 & 0 & -z\frac{\partial}{\partial x} & f(z) & 0 \\ 0 & 1 & -z\frac{\partial}{\partial y} & 0 & f(z) \\ 0 & 0 & 1 & 0 & 0 \end{bmatrix} \begin{Bmatrix} u_0(x,y,t) \\ v_0(x,y,t) \\ w_0(x,y,t) \\ \varphi_x(x,y,t) \\ \varphi_y(x,y,t) \end{Bmatrix} \tag{9}$$

where u_0, v_0 and w_0 denote the linear displacements of the middle surface of the plate. φ_x, φ_y are the cross-sectional rotations about the y and x directions, and $f(z)$ are Reddy shear strain functions [29].

The relationship between strain and displacement can be expressed as follows:

$$\varepsilon_x = \frac{\partial \mu}{\partial x} = \frac{\partial \mu_0}{\partial x} - z\frac{\partial^2 w_0}{\partial x^2} + f(z)\frac{\partial \theta_x}{\partial x} = \varepsilon_x^0 + z\varepsilon_x^b + f(z)\varepsilon_x^s \tag{10a}$$

$$\varepsilon_y = \frac{\partial v}{\partial y} = \frac{\partial v_0}{\partial y} - z\frac{\partial^2 w_0}{\partial y^2} + f(z)\frac{\partial \theta_y}{\partial y} = \varepsilon_y^0 + z\varepsilon_y^b + f(z)\varepsilon_y^s \tag{10b}$$

$$\gamma_{yz} = \frac{\partial v}{\partial z} + \frac{\partial w}{\partial y} = f'(z)\theta_y = f'(z)\gamma_{yz}^0 \tag{10c}$$

$$\gamma_{xz} = \frac{\partial w}{\partial x} + \frac{\partial u}{\partial z} = f'(z)\theta_x = f'(z)\gamma_{xz}^0 \tag{10d}$$

$$\begin{aligned} \gamma_{xy} &= \frac{\partial u}{\partial y} + \frac{\partial v}{\partial x} \\ &= \left(\frac{\partial u_0}{\partial y} + \frac{\partial v_0}{\partial x}\right) - z\frac{2\partial^2 w_0}{\partial x \partial y} + f(z)\left(\frac{\partial \theta_x}{\partial y} + \frac{\partial \theta_y}{\partial x}\right) \\ &= \gamma_{xy}^0 + z\gamma_{xy}^b + f(z)\gamma_{xy}^s \end{aligned} \tag{10e}$$

The resultant force and moment for the composite lattice sandwich panels are given as follows:

$$\begin{Bmatrix} N_x \\ N_y \\ N_{xy} \\ M_x \\ M_y \\ M_{xy} \\ S_x \\ S_y \\ S_{xy} \\ N_{yz} \\ N_{xz} \end{Bmatrix} = \begin{bmatrix} A_{11} & A_{12} & A_{16} & B_{11} & B_{12} & B_{16} & C_{11} & C_{12} & C_{16} & 0 & 0 \\ A_{12} & A_{22} & A_{26} & B_{12} & B_{22} & B_{26} & C_{12} & C_{22} & C_{26} & 0 & 0 \\ A_{16} & A_{26} & A_{66} & B_{16} & B_{26} & B_{66} & C_{12} & C_{22} & C_{26} & 0 & 0 \\ B_{11} & B_{12} & B_{16} & D_{11} & D_{12} & D_{16} & E_{11} & E_{12} & E_{16} & 0 & 0 \\ B_{12} & B_{22} & B_{26} & D_{12} & D_{22} & D_{26} & E_{12} & E_{22} & E_{26} & 0 & 0 \\ B_{16} & B_{26} & B_{66} & D_{16} & D_{26} & D_{66} & E_{16} & E_{26} & E_{66} & 0 & 0 \\ C_{11} & C_{12} & C_{16} & E_{11} & E_{12} & E_{16} & F_{11} & F_{12} & F_{16} & 0 & 0 \\ C_{12} & C_{22} & C_{26} & E_{12} & E_{22} & E_{26} & F_{12} & F_{22} & F_{26} & 0 & 0 \\ C_{16} & C_{26} & C_{66} & E_{16} & E_{26} & E_{66} & F_{16} & F_{26} & F_{66} & 0 & 0 \\ 0 & 0 & 0 & 0 & 0 & 0 & 0 & 0 & 0 & G_{44} & G_{45} \\ 0 & 0 & 0 & 0 & 0 & 0 & 0 & 0 & 0 & G_{45} & G_{55} \end{bmatrix} \begin{Bmatrix} \varepsilon_x^0 \\ \varepsilon_y^0 \\ \gamma_{xy}^0 \\ \varepsilon_x^b \\ \varepsilon_y^b \\ \gamma_{xy}^b \\ \varepsilon_x^s \\ \varepsilon_y^s \\ \gamma_{xy}^s \\ \gamma_{yz}^0 \\ \gamma_{xz}^0 \end{Bmatrix} \tag{11}$$

where N_i, M_i and S_i, are the total force and moment resultants. It is noted that due to the lattice core material being equivalent to isotropic material, G_{45} in Eq. (11) is equal to 0.

It is assumed that only bending deformation is considered for the top and bottom panels and only shear deformation is considered for the lattice core [27] [28]. Therefore, the stiffness coefficients are defined as:

$$\left(A_{ij}, B_{ij}, C_{ij}, D_{ij}, E_{ij}, F_{ij}\right) = \int_{h_c/2}^{h_c/2+h_f} Q_{ij}\left\{1, z, f(z), z^2, f(z)z, f^2(z)\right\}dz + \int_{-h_c/2-h_f}^{-h_c/2} Q_{ij}\left\{1, z, f(z), z^2, f(z)z, f^2(z)\right\}dz$$

$$G_{ij} = \int_{-h_c/2}^{h_c/2} Q_{ij}\left[f'(z)\right]^2 dz \tag{12}$$

The strain energy U_s of the composite lattice sandwich panels are expressed as:

$$\begin{aligned} U_s = \int_0^a \int_0^b \{ & A_{11}\varepsilon_x^0\varepsilon_x^0 + 2A_{12}\varepsilon_x^0\varepsilon_y^0 + 2A_{16}\varepsilon_x^0\gamma_{xy}^0 + 2B_{11}\varepsilon_x^0\varepsilon_x^b + 2B_{12}\varepsilon_x^0\varepsilon_y^b + 2B_{16}\varepsilon_x^0\gamma_{xy}^b \\ & + 2C_{11}\varepsilon_x^0\varepsilon_x^s + 2C_{12}\varepsilon_x^0\varepsilon_y^s + 2C_{16}\varepsilon_x^0\gamma_{xy}^s + 2B_{12}\varepsilon_x^b\varepsilon_y^0 + 2B_{16}\varepsilon_x^b\gamma_{xy}^0 + D_{11}\varepsilon_x^b\varepsilon_x^b + 2D_{12}\varepsilon_x^b\varepsilon_y^b \\ & + 2D_{16}\varepsilon_x^b\gamma_{xy}^b + 2E_{11}\varepsilon_x^b\varepsilon_x^s + 2E_{12}\varepsilon_x^b\varepsilon_y^s + 2E_{16}\varepsilon_x^b\gamma_{xy}^s + 2C_{12}\varepsilon_x^s\varepsilon_y^0 + 2C_{16}\varepsilon_x^s\varepsilon_{xy}^0 + 2E_{12}\varepsilon_x^s\varepsilon_y^b \\ & + 2E_{16}\varepsilon_x^s\gamma_{xy}^b + F_{11}\varepsilon_x^s\varepsilon_x^s + 2F_{12}\varepsilon_x^s\varepsilon_y^s + 2F_{16}\varepsilon_x^s\gamma_{xy}^s + A_{22}\varepsilon_y^0\varepsilon_y^0 + 2A_{26}\varepsilon_y^0\gamma_{xy}^0 + 2B_{22}\varepsilon_y^0\varepsilon_y^b \\ & + 2B_{26}\varepsilon_y^0\gamma_{xy}^b + 2C_{22}\varepsilon_y^0\varepsilon_y^s + 2C_{26}\varepsilon_y^0\gamma_{xy}^s + 2B_{26}\varepsilon_y^b\gamma_{xy}^0 + D_{22}\varepsilon_y^b\varepsilon_y^b + 2D_{26}\varepsilon_y^b\gamma_{xy}^b + 2E_{22}\varepsilon_y^b\varepsilon_y^s \\ & + 2E_{26}\varepsilon_y^b\gamma_{xy}^s + 2C_{26}\varepsilon_y^s\gamma_{xy}^0 + 2E_{26}\varepsilon_y^s\gamma_{xy}^b + F_{22}\varepsilon_y^s\varepsilon_y^s + 2F_{26}\varepsilon_y^s\gamma_{xy}^s + A_{66}\gamma_{xy}^0\gamma_{xy}^0 + 2B_{66}\gamma_{xy}^0\gamma_{xy}^b \\ & + 2C_{66}\gamma_{xy}^0\gamma_{xy}^s + D_{66}\gamma_{xy}^b\gamma_{xy}^b + 2E_{66}\gamma_{xy}^b\gamma_{xy}^s + F_{66}\gamma_{xy}^s\gamma_{xy}^s + G_{55}\gamma_{xz}^0\gamma_{xz}^0 + G_{44}\gamma_{yz}^0\gamma_{yz}^0 \}dxdy \end{aligned} \tag{13}$$

Substituting Eq. (10) into Eq. (13), the differential form of the strain energy can be rewritten as:

$$
\begin{aligned}
U_s = \int_0^a \int_0^b \{ & A_{11}\frac{\partial u_0}{\partial x}\frac{\partial u_0}{\partial x} + 2A_{12}\frac{\partial u_0}{\partial x}\frac{\partial v_0}{\partial y} + 2A_{16}\frac{\partial u_0}{\partial x}\left(\frac{\partial u_0}{\partial y} + \frac{\partial v_0}{\partial x}\right) \\
& -2B_{11}\frac{\partial u_0}{\partial x}\frac{\partial^2 w_0}{\partial x^2} - 2B_{12}\frac{\partial u_0}{\partial x}\frac{\partial^2 w_0}{\partial y^2} - 4B_{16}\frac{\partial u_0}{\partial x}\frac{\partial^2 w_0}{\partial x \partial y} + 2C_{11}\frac{\partial u_0}{\partial x}\frac{\partial \theta_x}{\partial x} \\
& +2C_{12}\frac{\partial u_0}{\partial x}\frac{\partial \theta_y}{\partial y} + 2C_{16}\frac{\partial u_0}{\partial x}\left(\frac{\partial \theta_x}{\partial y} + \frac{\partial \theta_y}{\partial x}\right) - 2B_{12}\frac{\partial^2 w_0}{\partial x^2}\frac{\partial^2 v_0}{\partial y^2} \\
& -2B_{16}\frac{\partial^2 w_0}{\partial x^2}\left(\frac{\partial u_0}{\partial y} + \frac{\partial v_0}{\partial x}\right) + D_{11}\frac{\partial^2 w_0}{\partial x^2}\frac{\partial^2 w_0}{\partial x^2} + 2D_{12}\frac{\partial^2 w_0}{\partial x^2}\frac{\partial^2 w_0}{\partial y^2} \\
& +4D_{16}\frac{\partial^2 w_0}{\partial x^2}\frac{\partial^2 w_0}{\partial x \partial y} - 2E_{11}\frac{\partial^2 w_0}{\partial x^2}\frac{\partial \theta_x}{\partial x} - 2E_{12}\frac{\partial^2 w_0}{\partial x^2}\frac{\partial \theta_y}{\partial y} \\
& -2E_{16}\frac{\partial^2 w_0}{\partial x^2}\left(\frac{\partial \theta_x}{\partial y} + \frac{\partial \theta_y}{\partial x}\right) + 2C_{12}\frac{\partial \theta_x}{\partial x}\frac{\partial v_0}{\partial y} + 2C_{16}\frac{\partial \theta_x}{\partial x}\left(\frac{\partial u_0}{\partial y} + \frac{\partial v_0}{\partial x}\right) \\
& -2E_{12}\frac{\partial \theta_x}{\partial x}\frac{\partial^2 w_0}{\partial y^2} - 4E_{16}\frac{\partial \theta_x}{\partial x}\frac{\partial^2 w_0}{\partial x \partial y} + F_{11}\frac{\partial \theta_x}{\partial x}\frac{\partial \theta_x}{\partial x} + 2F_{12}\frac{\partial \theta_x}{\partial x}\frac{\partial \theta_y}{\partial y} \\
& +2F_{16}\frac{\partial \theta_x}{\partial x}\left(\frac{\partial \theta_x}{\partial y} + \frac{\partial \theta_y}{\partial x}\right) + A_{22}\frac{\partial v_0}{\partial y}\frac{\partial v_0}{\partial y} + 2A_{26}\frac{\partial v_0}{\partial y}\left(\frac{\partial u_0}{\partial y} + \frac{\partial v_0}{\partial x}\right) \\
& -2B_{22}\frac{\partial v_0}{\partial y}\frac{\partial^2 w_0}{\partial y^2} - 4B_{26}\frac{\partial v_0}{\partial y}\frac{\partial^2 w_0}{\partial x \partial y} + 2C_{22}\frac{\partial v_0}{\partial y}\frac{\partial \theta_y}{\partial y} \\
& +2C_{26}\frac{\partial v_0}{\partial y}\left(\frac{\partial \theta_x}{\partial y} + \frac{\partial \theta_y}{\partial x}\right) - 2B_{26}\frac{\partial^2 w_0}{\partial y^2}\left(\frac{\partial u_0}{\partial y} + \frac{\partial v_0}{\partial x}\right) + D_{22}\frac{\partial^2 w_0}{\partial y^2}\frac{\partial^2 w_0}{\partial y^2} \\
& +4D_{26}\frac{\partial^2 w_0}{\partial y^2}\frac{\partial^2 w_0}{\partial x \partial y} - 2E_{22}\frac{\partial^2 w_0}{\partial y^2}\frac{\partial \theta_y}{\partial y} - 2E_{26}\frac{\partial^2 w_0}{\partial y^2}\left(\frac{\partial \theta_x}{\partial y} + \frac{\partial \theta_y}{\partial x}\right) \\
& +2C_{26}\frac{\partial \theta_y}{\partial y}\left(\frac{\partial u_0}{\partial y} + \frac{\partial v_0}{\partial x}\right) - 4E_{26}\frac{\partial \theta_y}{\partial y}\frac{\partial^2 w_0}{\partial x \partial y} + F_{22}\frac{\partial \theta_y}{\partial y}\frac{\partial \theta_y}{\partial y} \\
& +2F_{26}\frac{\partial \theta_y}{\partial y}\left(\frac{\partial \theta_x}{\partial y} + \frac{\partial \theta_y}{\partial x}\right) + A_{66}\left(\frac{\partial^2 u_0}{\partial y^2} + 2\frac{\partial u_0}{\partial y}\frac{\partial v_0}{\partial y} + \frac{\partial^2 v_0}{\partial x^2}\right) \\
& -4B_{66}\left(\frac{\partial u_0}{\partial y} + \frac{\partial v_0}{\partial x}\right)\frac{\partial^2 w_0}{\partial x \partial y} + 2C_{66}\left(\frac{\partial u_0}{\partial y} + \frac{\partial v_0}{\partial x}\right)\left(\frac{\partial \theta_x}{\partial y} + \frac{\partial \theta_y}{\partial x}\right) \\
& +4D_{66}\frac{\partial^2 w_0}{\partial x \partial y}\frac{\partial^2 w_0}{\partial x \partial y} - 4E_{66}\frac{\partial^2 w_0}{\partial x \partial y}\left(\frac{\partial \theta_x}{\partial y} + \frac{\partial \theta_y}{\partial x}\right) \\
& +F_{66}\left(\frac{\partial \theta_x}{\partial y} + \frac{\partial \theta_y}{\partial x}\right)\left(\frac{\partial \theta_x}{\partial y} + \frac{\partial \theta_y}{\partial x}\right) + G_{55}\theta_x\theta_x + G_{44}\theta_y\theta_y \} dxdy
\end{aligned} \tag{14}
$$

The boundary spring potential energy U_{sp} can be given as:

$$
\begin{aligned}
U_{sp} = & \frac{1}{2}\int_{-h/2}^{h/2}\int_0^b \begin{Bmatrix} \left[k_{x0}^u u_0^2 + k_{x0}^v v_0^2 + k_{x0}^w w_0^2 + k_{x0}^x \varphi_x^2 + k_{x0}^y \varphi_y^2\right]_{x=0} \\ \left[k_{xa}^u u_0^2 + k_{xa}^v v_0^2 + k_{xa}^w w_0^2 + k_{xa}^x \varphi_x^2 + k_{xa}^y \varphi_y^2\right]_{x=a} \end{Bmatrix} dydz \\
& + \frac{1}{2}\int_{-h/2}^{h/2}\int_0^a \begin{Bmatrix} \left[k_{y0}^u u_0^2 + k_{y0}^v v_0^2 + k_{y0}^w w_0^2 + k_{y0}^x \varphi_x^2 + k_{y0}^y \varphi_y^2\right]_{y=0} \\ \left[k_{ya}^u u_0^2 + k_{ya}^v v_0^2 + k_{ya}^w w_0^2 + k_{ya}^x \varphi_x^2 + k_{ya}^y \varphi_y^2\right]_{y=a} \end{Bmatrix} dxdz
\end{aligned} \tag{15}
$$

Moreover, the kinetic energy T of the composite lattice sandwich panels can be determined:

$$
\begin{aligned}
T &= \frac{1}{2}\iiint_V \rho(z)\left[(u_{,t})^2 + (v_{,t})^2 + (w_{,t})^2\right] dV \\
&= \frac{1}{2}\int_0^a \int_0^b \begin{bmatrix} I_0\left(u_{0,t}^2 + v_{0,t}^2 + w_{0,t}^2\right) - 2I_1\left(u_{0,t}w_{0,x,t} + v_{0,t}w_{0,y,t}\right) \\ +2I_2\left(u_{0,t}\theta_{x,t} + v_{0,t}\theta_{y,t}\right) \\ -2I_3\left(w_{0,x,t}\theta_{x,t} + w_{0,y,t}\theta_{y,t}\right) + I_4\left(\theta_{x,t}^2 + \theta_{y,t}^2\right) + I_5 w_{0,x,t}^2 \end{bmatrix} dxdy
\end{aligned} \tag{16}
$$

where the mass inertias (I_0, I_1, I_2, I_3, I_4, I_5, I_6) are defined as:

$$
\left(I_0, I_1, I_2, I_3, I_4, I_5, I_6\right) = \int_{-h/2}^{h/2}\left[1, z, f(z), zf(z), f^2(z), z^2\right]\rho(z)dz \tag{17}
$$

The Lagrangian energy function L of the sandwich composite lattice panels can be obtained as:

$$
L = U_s + U_{sp} - T \tag{18}
$$

In order to simulate the arbitrary boundary conditions, the improved Fourier series displacements are used to eliminate discontinuities of the displacements and their derivatives at the structural boundaries [25, 30]. The displacement functions of the composite lattice sandwich plates can be expressed as the follows:

$$
\begin{aligned}
u_0(x,y,t) = & \sum_{m=-2}^{-1}\sum_{n=-2}^{-1} A_{mn}^1 \sin(\lambda_m x)\sin(\lambda_n y) + \sum_{m=-2}^{-1}\sum_{n=0}^{N} A_{mn}^2 \sin(\lambda_m x)\cos(\lambda_n y) \\
& + \sum_{n=-2}^{-1}\sum_{m=0}^{M} A_{mn}^3 \cos(\lambda_m x)\sin(\lambda_n y) + \sum_{m=0}^{M}\sum_{n=0}^{N} A_{mn}^4 \cos(\lambda_m x)\cos(\lambda_n y)
\end{aligned} \tag{19a}
$$

$$
\begin{aligned}
v_0(x,y,t) = & \sum_{m=-2}^{-1}\sum_{n=-2}^{-1} B_{mn}^1 \sin(\lambda_m x)\sin(\lambda_n y) \\
& + \sum_{m=-2}^{-1}\sum_{n=0}^{N} B_{mn}^2 \sin(\lambda_m x)\cos(\lambda_n y) \\
& + \sum_{n=-2}^{-1}\sum_{m=0}^{M} B_{mn}^3 \cos(\lambda_m x)\sin(\lambda_n y) \\
& + \sum_{m=0}^{M}\sum_{n=0}^{N} B_{mn}^4 \cos(\lambda_m x)\cos(\lambda_n y)
\end{aligned} \tag{19b}
$$

$$
\begin{aligned}
w_0(x,y,t) = & \sum_{m=-2}^{-1}\sum_{n=-2}^{-1} C_{mn}^1 \sin(\lambda_m x)\sin(\lambda_n y) \\
& + \sum_{m=-2}^{-1}\sum_{n=0}^{N} C_{mn}^2 \sin(\lambda_m x)\cos(\lambda_n y) \\
& + \sum_{n=-2}^{-1}\sum_{m=0}^{M} C_{mn}^3 \cos(\lambda_m x)\sin(\lambda_n y) \\
& + \sum_{m=0}^{M}\sum_{n=0}^{N} C_{mn}^4 \cos(\lambda_m x)\cos(\lambda_n y)
\end{aligned} \tag{19c}
$$

$$
\begin{aligned}
\theta_x(x,y,t) = & \sum_{m=-2}^{-1}\sum_{n=-2}^{-1} D_{mn}^1 \sin(\lambda_m x)\sin(\lambda_n y) \\
& + \sum_{m=-2}^{-1}\sum_{n=0}^{N} D_{mn}^2 \sin(\lambda_m x)\cos(\lambda_n y) \\
& + \sum_{n=-2}^{-1}\sum_{m=0}^{M} D_{mn}^3 \cos(\lambda_m x)\sin(\lambda_n y) \\
& + \sum_{m=0}^{M}\sum_{n=0}^{N} D_{mn}^4 \cos(\lambda_m x)\cos(\lambda_n y)
\end{aligned} \tag{19d}
$$

$$
\begin{aligned}
\theta_y(x,y,t) = & \sum_{m=-2}^{-1}\sum_{n=-2}^{-1} E_{mn}^1 \sin(\lambda_m x)\sin(\lambda_n y) \\
& + \sum_{m=-2}^{-1}\sum_{n=0}^{N} E_{mn}^2 \sin(\lambda_m x)\cos(\lambda_n y) \\
& + \sum_{n=-2}^{-1}\sum_{m=0}^{M} E_{mn}^3 \cos(\lambda_m x)\sin(\lambda_n y) \\
& + \sum_{m=0}^{M}\sum_{n=0}^{N} E_{mn}^4 \cos(\lambda_m x)\cos(\lambda_n y)
\end{aligned} \tag{19e}
$$

where $\lambda_m = m\pi/a$, $\lambda_n = n\pi/b$, M and N represent the number of truncations. In addition,A_{mn}^k,B_{mn}^k,C_{mn}^k,D_{mn}^k and E_{mn}^k ($k = 1,2,3,4$) denote the coefficients of two-dimensional Fourier series.

Moreover, by substituting Eqs. (14), (15), (16), (19a), (19b), (19c), (19d) and (19e) into Eq. (18) and solving for the partial derivatives of the Lagrange energy function L with respect to the unknown coefficients, the following expression can be obtained:

$$\frac{\partial L}{\partial \psi_k} = 0, \psi_k = A_{mn}^k, B_{mn}^k, C_{mn}^k, D_{mn}^k, E_{mn}^k \tag{20}$$

The system of governing equations is expressed in form of eigenvalue equation:

$$(K - w^2 M)q = 0 \tag{21}$$

where $q = [A_{mn}^k, B_{mn}^k, C_{mn}^k, D_{mn}^k, E_{mn}^k]^T$ is the coefficient vector, the stiffness matrix K and the mass matrix M can be given as:

$$K = \begin{bmatrix} K_{uu} & K_{uv} & K_{uw} & K_{ux} & K_{uy} \\ K_{vu} & K_{vv} & K_{vw} & K_{vx} & K_{vy} \\ K_{wu} & K_{wv} & K_{ww} & K_{wx} & K_{wy} \\ K_{xu} & K_{xv} & K_{xw} & K_{xx} & K_{xy} \\ K_{yu} & K_{yv} & K_{yw} & K_{yx} & K_{yy} \end{bmatrix} \tag{22}$$

$$T = \begin{bmatrix} T_{uu} & 0 & T_{uw} & T_{ux} & 0 \\ 0 & T_{vv} & T_{vw} & 0 & T_{vy} \\ T_{wu} & T_{wv} & T_{ww} & T_{wx} & T_{wy} \\ T_{xu} & 0 & T_{xw} & T_{xx} & 0 \\ 0 & T_{yv} & T_{yw} & 0 & T_{yy} \end{bmatrix} \tag{23}$$

The natural vibration frequencies w and their corresponding vector of coefficients $[A_{mn}^k, B_{mn}^k, C_{mn}^k, D_{mn}^k, E_{mn}^k]^T$ can be obtained after solving the Eq. (21). Finally, by substituting these coefficients to Eqs. (19a), (19b), (19c), (19d) and (19e), the mode shapes can be determined. The flow chart of the current procedure is shown in Fig. 5.

Numerical Results and Discussion

The convergence and accuracy of the proposed method needs to be verified before conducting the kinetic characterization. In this paper, the material properties for all arithmetic examples are: $E_1 = 150$ GPa, $E_2 = 10$ GPa, $\mu_{12} = 0.3$, $\mu_{21} = \mu_{12}E_1/E_2$, $\rho = 1500$ kg/m^3 without otherwise specified. Assuming the Poisson's ratio for the trapezoidal lattice core of 0.3. In addition, the non-dimensional frequency parameter $\Omega = wL_a^2/h\sqrt{\rho_0/E_2}$ is used for discussion. In order to minimize research variables, uniform unidirectional plies were employed for the upper laminate, lower laminate, and trapezoidal lattice core, denoted as A-B-C. For instance, the lamination scheme 90–0-90 signifies the orientation of the upper and lower laminates at 90 degrees, and the core material at 0 degrees. The orientation of the 0-degree plies for each panel is indicated as depicted in Fig. 1. The arbitrary boundary conditions can be achieved by setting various stiffness values of the linear and rotational artificial springs [31]: (1) Free BC: $K_u = K_v = K_w = K_x = K_y = 0$, (2) Clamped BC: $K_u = K_v = K_w = K_x = K_y = 10^{14}$, (3) Simply-supported BC ($x = 0$, $x = L_a$): $K_u = K_x = 0$, $K_v = K_w = K_y = 10^{14}$, (4) Simply-supported BC ($y = 0$, $y = L_b$): $K_v = K_y = 0$, $K_x = K_w = K_x = 10^{14}$, (5) Elastic BC ($E_1$): $K_u = K_v = K_w = 10^8$, $K_x = K_y = 10^{14}$, (6) Elastic BC (E_2): $K_u = K_v = K_w = 10^{14}$, $K_x = K_y = 10^8$, (7) Elastic BC (E_3): $K_u = K_v = K_w = K_x = K_y = 10^8$.

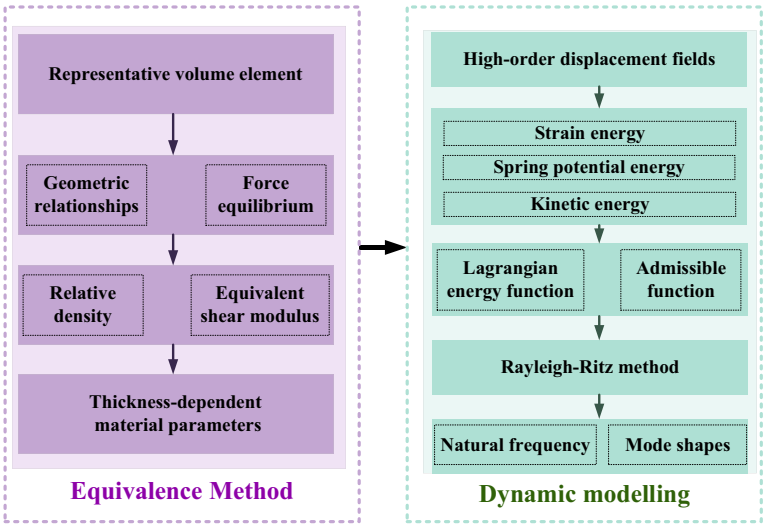

Fig. 5 Flow-chart for the current procedure

Table 1 Convergence of frequency parameters of the trapezoidal lattice sandwich composite panels

M×N	Mode number					
	1	2	3	4	5	6
2×2	2.864	9.144	11.354	21.937	24.622	40.341
4×4	2.855	4.327	6.840	8.006	13.694	16.076
6×6	2.782	4.152	5.704	5.882	6.652	7.959
8×8	2.757	4.074	5.520	5.717	6.422	7.666
10×10	2.746	4.032	5.457	5.654	6.334	7.562
12×12	2.740	4.007	5.430	5.620	6.207	7.495
14×14	2.735	3.993	5.415	5.599	6.274	7.440
16×16	2.732	3.999	5.429	5.585	6.259	7.457
18×18	2.730	3.996	5.423	5.573	6.250	7.433
20×20	2.728	3.989	5.418	5.561	6.244	7.416

Table 2 Non-dimensional vibration frequency for the composite sandwich panels in Hz

Mode	Exp. [32]	Ref. [32]	Ref. [33]	Ref. [34]	Present
1	-	23	23.59	23.63	23.32
2	45	45	45.84	46.1	44.75
3	69	71	73.09	74.2	71.28
4	78	80	84.14	86.19	80.49
5	92	91	94.03	96.36	92.49

Table 3 Non-dimensional frequencies of sandwich plates with trapezoidal lattice core

	f_1	f_2	f_3
Present	2.746	4.032	5.654
FEM	2.765	4.325	6.064
Error (%)	0.68	6.77	6.76

Convergence and Validation

In this section, the convergence of the model is first assessed by calculating and comparing the dimensionless frequencies at different truncation numbers M and N, as shown in Table 1. The truncated values range from 2×2 to 20×20. The geometric parameters of the sandwich lattice plates under CCCC boundary condition are listed: $L_a = 0.9$ m, $L_b = 0.9$ m, $h = 0.012$ m, $\theta = 60°$, and the lamination scheme is 0–0-0. It can be seen from Table 1 that the dimensionless frequency of each order tends to stabilize as the truncation value increases. Therefore, in order to meet the requirements of the accuracy and the computational efficiency, the truncation value in this paper is $M = N = 10$.

In order to verify the accuracy of the proposed model for the composite sandwich panels, the present results are compared with those in the available literature, as shown in Table 2. The geometrical and material properties are used [32]: $a = 1.83$ m, $b = 1.22$ m, $h_s = 4.06 \times 10^{-4}$ m, $h_c = 0.0064$ m. For face layers: $E_1 = E_2 = 68.9$ GPa, $\nu_{12} = 0.30$, $\rho_s = 2.77 \times 10^3$ kg/m^3. For core layer: $G_{13} = 0.134$ GPa, $G_{23} = 0.052$ GPa, $\rho_c = 0.122 \times 10^3$ kg/m^3. The results are compared with the experimental results and analytical solutions proposed by Raville et al. [32], Chandrashekhar et al. [33] and Nayak et al. [34]. It can be seen that the obtained results are closer to the experimental and analytical results provided by Raville et al. [32].

To further demonstrate the accuracy and correctness of the proposed method, the comparison of the non-dimensional frequencies with vibration modes in the same direction is also given in Table 3. The geometric parameters of the trapezoidal lattice sandwich panels under simply-supported boundary condition are given: $L_a = 0.9$ m, $L_b = 0.9$ m, $h = 0.012$ m, $\theta = 60°$, and the lamination scheme is 0–0-0. The results are obtained based on the present method and FEM. It shows that the maximum error between the present method and the FEM model is around 6%. Considering the highly anisotropic nature of the fiber-reinforced lattice core and the results can also prove the accuracy of the present method.

Table 4 shows the variation in the first eight vibration frequencies of the composite lattice sandwich panels with various boundary conditions and different geometric constants. The geometric constants used in this case are: $h = 0.012$ m, $\theta = 60°$, and the lamination scheme is 0–0–0. The results show that the vibration frequencies of the composite lattice sandwich panel with $a/b = 2$ is the highest among all cases. This is because the layup at this point determines the maximum bending stiffness in the length direction and corresponds to the maximum intrinsic frequency. It is worth noting that the vibration frequencies for the composite lattice sandwich panels under the boundary condition of CCCC are the highest and the vibration frequencies for the composite lattice sandwich panels under the boundary condition of $E_1E_2E_1E_2$ are always higher than those under the boundary condition of SSSS irrespective of the aspect ratio a/b. This indicates that the frequency of the trapezoidal lattice panel is positively correlated with the boundary stiffness

Table 4 Variation in the vibration frequency for the composite lattice sandwich panels with various boundary conditions and geometric constants

Boundary constraints	*a*/*b*	Mode number							
		1	2	3	4	5	6	7	8
CCCC	1	2.746	4.032	5.457	5.654	6.334	7.562	7.601	9.210
	0.5	2.351	2.727	3.279	3.984	4.744	5.090	5.448	5.708
	2	4.219	6.456	7.954	9.517	10.300	12.558	12.584	13.736
SSSS	1	2.184	3.445	4.271	4.977	5.092	6.307	6.694	7.635
	0.5	1.768	2.184	2.768	3.448	4.051	4.196	4.271	4.624
	2	3.445	5.092	6.680	7.806	8.175	10.245	10.646	11.534
$E_1E_2E_1E_2$	1	2.738	4.025	5.418	5.650	6.295	7.532	7.598	9.190
	0.5	2.343	2.718	3.271	3.977	4.738	5.061	5.409	5.704
	2	4.212	6.415	7.950	9.497	10.209	12.528	12.556	13.727

coefficient. In addition, it is clear that the aspect ratio *a*/*b* becomes more sensitive to the frequency changes as the mode order increases.

The effects of the lamination schemes on the first five non-dimensional frequencies of the composite lattice sandwich panels with different boundary and geometric conditions are shown in Table 5. The geometric constants of composite lattice sandwich panels with different lamination schemes (90–0–90, 45–0–45 and 45–90–45) are used as follows: $a=0.9$ m, $b=0.9$ m, $h=0.012$ m. The tilt angle θ varies from 30° to 60° and the interval angle of a step is 15° in the study. From the figure, it can be seen that the vibration frequencies of the composite lattice sandwich panels decrease with the tilt angle θ. And the vibration frequencies of the composite lattice sandwich panels under the boundary condition of CCCC are the highest irrespective of tilt angle θ and lamination scheme. Besides, the vibration frequencies of lattice sandwich panels with 45–0–45 lamination scheme are the highest and the those with 45–90–45 are the lowest. Based on the above analysis, it means that the vibration frequencies of the composite lattice sandwich panels strongly depend on the boundary conditions and geometrical parameters.

The effect of aspect ratios on the first four vibration pattern of the lattice sandwich plate with $a=0.9$ m, $h=0.012$ m, $\theta=60°$ and SSSS boundary condition is also investigated, as shown in Fig. 6. The lamination scheme is 0–0–0. From Fig. 6, it can be seen that for the square plate, the 2nd and 3rd order vibration patterns are similar and just the vibration frequencies are different. For the cases of $a/b=0.5$ and $a/b=2$, there is mainly a difference between the third and fourth orders, which is mainly due to the different elastic modules of the upper and lower composite panels in the x and y directions. This indicates that the aspect ratio and the fiber orientation have a great influence on the vibration pattern of the lattice sandwich panels.

Figure 7 shows the effect of the boundary conditions and the tilt angle θ on the frequency parameters of the composite

Table 5 The first five frequency parameters for the composite lattice sandwich panels with various boundary, geometric conditions and lamination schemes

θ (°)	Mode	[90 0 90]		[45 0 45]		[45 90 45]	
		CCCC	SSSS	CCCC	SSSS	CCCC	SSSS
30	1	3.294	2.769	3.290	3.284	1.601	1.596
	2	4.971	4.398	5.301	5.306	2.631	2.631
	3	6.225	5.101	5.714	5.716	3.441	3.445
	4	6.987	6.179	7.082	7.082	3.739	3.731
	5	7.358	6.315	8.242	8.243	5.034	5.038
45	1	3.228	2.699	3.217	3.202	1.588	1.577
	2	4.856	4.283	5.186	5.191	2.612	2.619
	3	6.127	4.997	5.606	5.610	3.427	3.429
	4	6.823	6.044	6.933	6.921	3.717	3.709
	5	7.229	6.149	8.091	8.088	5.010	5.012
60	1	2.746	2.184	2.696	2.690	1.506	1.499
	2	4.029	3.443	4.353	5.864	2.489	2.485
	3	5.460	4.273	4.849	5.870	3.340	3.337
	4	5.646	4.972	5.870	7.030	3.574	3.572
	5	6.335	5.092	7.028	7.556	4.850	4.850

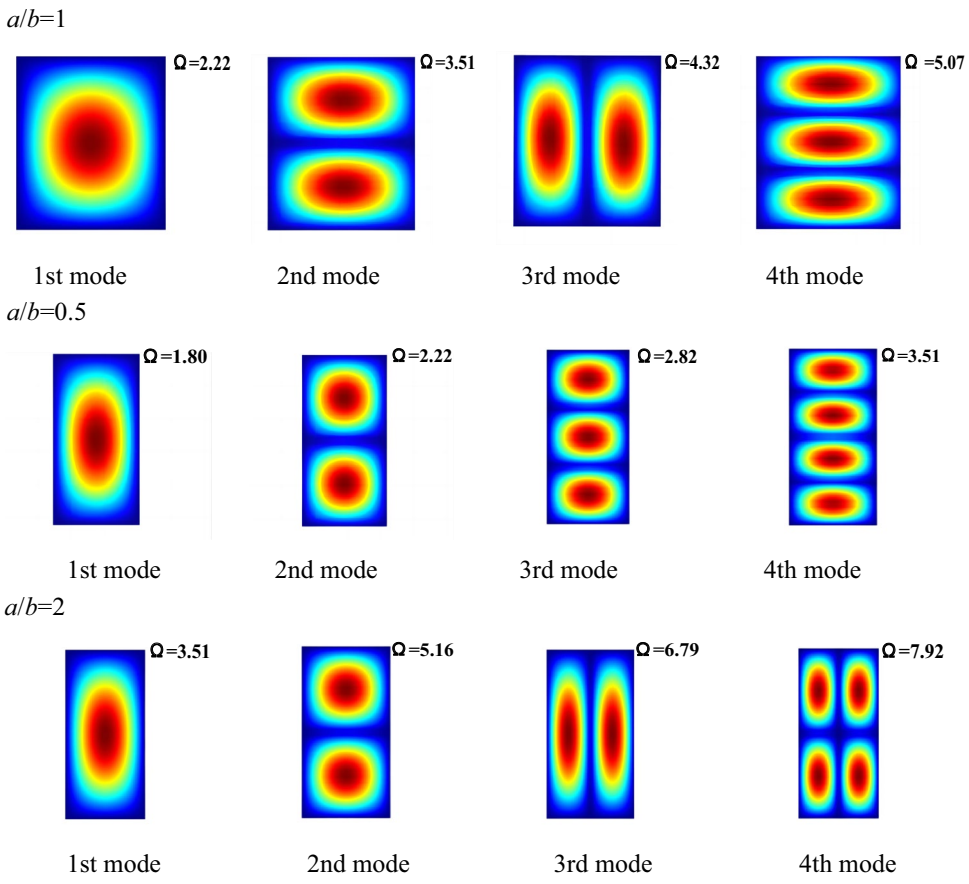

Fig. 6 Mode shapes for the composite lattice sandwich panels with various aspect ratios under the boundary condition of the SSSS

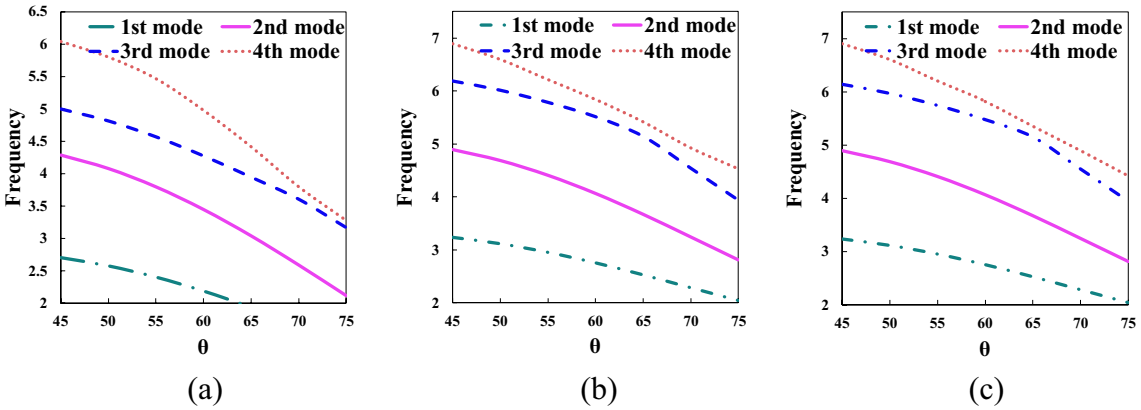

Fig. 7 The first four frequency parameters of the composite lattice sandwich panels with different boundary conditions and tilt angle θ: **a** SSSS; **b** CE_3CE_3;**c** $E_1E_2E_1E_2$

lattice sandwich panels ($a=0.9$ m, $b=0.9$ m, $h=0.012$ m). The lamination schemes are 0–0-0 and the tilt angle θ is varied from 45° to 75°. According to Fig. 7, it is observed that the frequency parameters decrease as the tilt angle θ increases, and the trends of the frequency curves with different vibration modes are similar. In addition, there is a

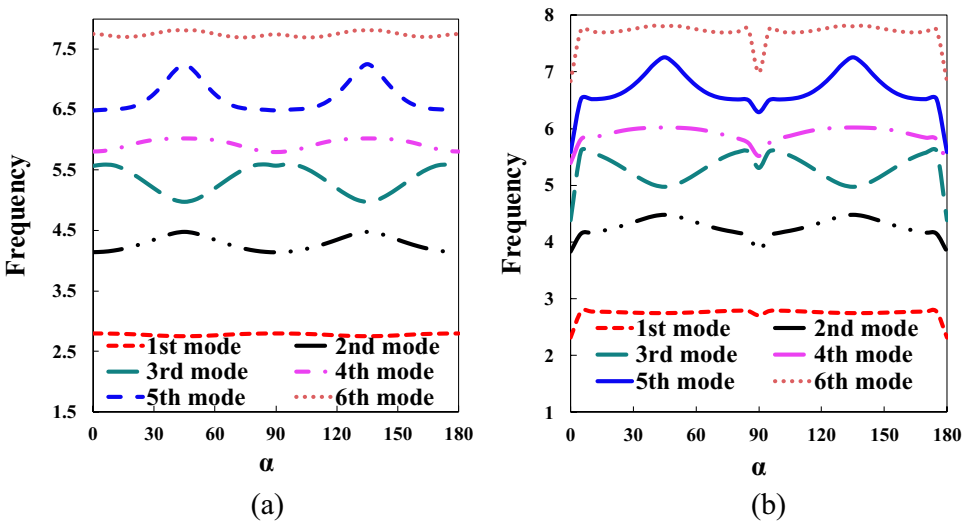

Fig. 8 Vibration frequency versus α for the composite lattice sandwich panels with different boundary conditions: **a** CCCC; **b** SCSC

small difference between the frequency curves of CE_3CE_3 and those of $E_1E_2E_1E_2$, while the frequencies of lattice sandwich plate with SSSS boundary condition are the smallest among all boundary conditions.

Figure 8 shows the vibration frequencies of the composite lattice sandwich panels with the lamination schemes α-0-α and different boundary conditions. The fiber orientation α is varied from 0° to 180°. The results show that the frequency curves are symmetrical about 90 degrees and the trends of the frequency curves of each order are similar regardless of the boundary condition. When the boundary condition is the CCCC, the first and sixth order frequencies are insensitive to changes in fiber orientation, and the other order frequencies fluctuate with changes in fiber orientation. In addition, the 2nd, 4th, and 5th order frequencies reach their maximum values and the 3rd order frequency reaches its minimum value when the angles are 45 and 135 degrees. When the boundary condition is the SCSC, only the first order frequencies are insensitive to changes in fiber orientation. Moreover, the 2nd, 4th, 5th, and 6th order frequencies reach their maximum values and the 3rd order frequency reaches its minimum value when the angles are 45 and 135 degrees.

Conclusion

In this paper, a new equivalent method to predict thickness-dependent shear modulus and density of trapezoidal lattice composite cores, and the equivalent material properties are deduced based on the single-cell equivalence theory and the continuity assumption. The novelty of this work is that the proposed equivalent method can be used to calculate the equivalent material properties which are gradually changed in the thickness direction, while traditional method usually limits to the lattice core with a uniform cross-section. The higher order shear deformation theory is adopted to derive the strain energy and the kinetic energy of the lattice sandwich plate. The admissible displacement functions are expanded as improved Fourier series, and the unknown displacement coefficients are solved based on Rayleigh–Ritz method. The artificial springs are introduced to simulate the general boundary conditions. The main findings can be drawn as follows:

- The accuracy and convergence of the present method have been verified by comparing the obtained results with those of the literature and FEM ones. On this basis, the effects of boundary conditions, aspect ratio, tilt angle and lamination schemes on the vibration frequency are investigated.
- The comparative results illustrate that the effects of various geometric parameters and lamination schemes on the frequencies are significant, and the vibration frequency of the composite lattice sandwich panel increases with the increase of the aspect ratios, boundary stiffness coefficients and tilt angles. In addition, the aspect ratio becomes more sensitive to the variation of high frequency.
- Regardless of the boundary conditions, the frequency curves are symmetric about 90 degrees, and the frequencies of each order reach the maximum or minimum when the angles are 45 degrees and 135 degrees, respectively.
- The limitation of this study is that the current method is proposed for the sandwich plates with lattice core, which is not applicable to the those with honeycomb and corrugated core. In addition, future study would further investigate the effect of fiber orientation of composite lattice core and the distribution density of unit cell on the dynamic characteristics (including the free and forced vibration) of the lattice sandwich composite plates and shells.

Acknowledgements The work is supported by the National Natural Science Foundation of China (Grant Numbers: 12202324).

Data availability Data sharing is not applicable to this paper as no data sets were created or analyzed during the current investigation.

References

1. Zhu C, Li G, Ruan S, Yang J (2023) Structural intensity of laminated composite plates subjected to distributed force excitation. J Vib Eng Technol 11:2779–2791
2. Fang H, Liu Z, Lei M, Duan L (2022) A High-stiffness sandwich structure with a tristable core for low-frequency vibration isolation. J Vib Eng Technol 10:1989–2003
3. Gonenli C (2022) Effect of cut-out location on the dynamic behaviour of plate frame structures. J Vib Eng Technol 10:1599–1611
4. Xiao M, Liu X, Zhang Y, Gao L, Gao J, Chu S (2021) Design of graded lattice sandwich structures by multiscale topology optimization. Comput Method Appl M 384:13949
5. Bai L, Gong C, Chen X, Sun Y, Xin L, Pu H, Peng Y, Luo J (2020) Mechanical properties and energy absorption capabilities of functionally graded lattice structures: experiments and simulations. Int J Mech Sci 182:105735
6. Deshpande VS, Fleck NA, Ashby MF (2001) Effective properties of the octet-truss lattice material. J Mech Phys Solids 49:1747–1769
7. Hyun S, Karlsson AM, Torquato S, Evans AG (2003) Simulated properties of Kagomé and tetragonal truss core panels. Int J Solids Struct 40:6989–6998
8. Beiranvand H, Hosseini SAA (2022) New nonlinear first-order shear deformation beam model based on geometrically exact theory. J Vib Eng Technol 11:4187–4204
9. Zhang Z, Han B, Zhang Q, Jin F (2017) Free vibration analysis of sandwich beams with honeycomb-corrugation hybrid cores. Compos Struct 171:335–344
10. Lou J, Wang B, Ma L, Wu L (2013) Free vibration analysis of lattice sandwich beams under several typical boundary conditions. Acta Mech Solida Sin 26:458–467
11. Han Y, Wang P, Fan H, Sun F, Chen L, Fang D (2015) Free vibration of CFRC lattice-core sandwich cylinder with attached mass. Compos Sci Technol 118:226–235
12. Yifeng Z, Mingtao Z, Yujie Z, Zheng S (2023) Time- and frequency-domain vibration analysis of enhanced pyramid lattice sandwich plates using an equivalent downscaling model. Mater Today Commun 34:105268
13. Kwak S, Kim K, Jong G, Kim Y, Ri C (2021) A novel solution method for free vibration analysis of functionally graded arbitrary quadrilateral plates with hole. J Vib Eng Technol 9:1769–1787
14. Li H, Dong B, Zhao J, Zou Z, Zhao S, Wang Q, Han Q, Wang X (2022) Nonlinear free vibration of functionally graded fiber-reinforced composite hexagon honeycomb sandwich cylindrical shells. Eng Struct 263:114372
15. Seçgin A, Kara M (2019) Stochastic vibration analyses of laminated composite plates via a statistical moments-based methodology. J Vib Eng Technol 7:73–82
16. Zhang W, He LJ, Wang JF (2022) Content-dependent nonlinear vibration of composite plates reinforced with carbon nanotubes. J Vib Eng Technol 10:1253–1264
17. Banerjee R, Rout M, Karmakar A, Bose D (2023) Free vibration response of rotating hybrid composite conical shell under hygrothermal conditions. J Vib Eng Technol 11:1921–1938
18. Saiah B, Chiker Y, Bachene M, Attaf B, Guemana M (2023) Vibrational Behavior of Temperature-Dependent Piece-Wise Functionally Graded Polymeric Nanocomposite Plates Reinforced with Monolayer Graphene. J Vib Eng Technol
19. Raza A, Dwivedi K, Pathak H, Talha M (2023) Free Vibration of Porous Functionally Graded Plate with Crack Using Stochastic XFEM Approach. J Vib Eng Technol
20. Liu T, Zheng Y, Qian Y (2023) Frequency Change and Mode Shape Transformation in Free Vibration Analysis of Three-Phase Composite Thin Plate Under Different Boundary Conditions. J Vib Eng Technol
21. Li S, Yang J-S, Wu L-Z, Yu G-C, Feng L-J (2019) Vibration behavior of metallic sandwich panels with Hourglass truss cores. Mar Struct 63:84–98
22. Zhou Z, Chen M, Jia W, Xie K (2020) Free and forced vibration analyses of simply supported Z-reinforced sandwich structures with cavities through a theoretical approach. Compos Struct 243:112182
23. Li M, Du S, Li F, Jing X (2020) Vibration characteristics of novel multilayer sandwich beams: Modelling, analysis and experimental validations. Mech Syst Signal Pr 142:106799
24. Zhang H, Shi D, Wang Q (2017) An improved Fourier series solution for free vibration analysis of the moderately thick laminated composite rectangular plate with non-uniform boundary conditions. Int J Mech Sci 121:1–20
25. Qin B, Zhong R, Wu Q, Wang T, Wang Q (2019) A unified formulation for free vibration of laminated plate through Jacobi-Ritz method. Thin Wall Struct 144:106354
26. Li H, Hao YX, Zhang W, Liu LT, Yang SW, Wang DM (2021) Vibration analysis of porous metal foam truncated conical shells with general boundary conditions using GDQ. Compos Struct 269:114036
27. Xu G, Zeng T, Cheng S, Wang X, Zhang K (2019) Free vibration of composite sandwich beam with graded corrugated lattice core. Compos Struct 229:111466
28. Xu M, Qiu Z (2013) Free vibration analysis and optimization of composite lattice truss core sandwich beams with interval parameters. Compos Struct 106:85–95
29. Rj N (1984) A simple higher-order theory for laminated composite plates. J Appl Mech 51:745–752
30. Shao D, Hu S, Wang Q, Pang F (2017) An enhanced reverberation-ray matrix approach for transient response analysis of composite laminated shallow shells with general boundary conditions. Compos Struct 162:133–155
31. Kim K, Choe K, Kim S, Wang Q (2019) A modeling method for vibration analysis of cracked laminated composite beam of uniform rectangular cross-section with arbitrary boundary condition. Compos Struct 208:127–140
32. Raville ME, Ueng CES (1967) Determination of natural frequencies of vibration of a sandwich plate. Exp Mech 7:490–493
33. Chandrashekhar M, Ganguli R (2010) Nonlinear vibration analysis of composite laminated and sandwich plates with random material properties. Int J Mech Sci 52:874–891
34. Nayak AK, Moy SSJ, Shenoi RA (2002) Free vibration analysis of composite sandwich plates based on Reddy's higher-order theory. Compos Part B-Eng 33:505–519

Publisher's Note Springer Nature remains neutral with regard to jurisdictional claims in published maps and institutional affiliations.

Springer Nature or its licensor (e.g. a society or other partner) holds exclusive rights to this article under a publishing agreement with the author(s) or other rightsholder(s); author self-archiving of the accepted manuscript version of this article is solely governed by the terms of such publishing agreement and applicable law.